Supporting Information

Over 14% efficiency all-polymer solar cells enabled by a low bandgap polymer acceptor with low energy loss and efficient charge separation

Qunping Fan,[a] Qiaoshi An,[b] Yuanbao Lin,[d] Yuxin Xia,[e] Qian Li,[f] Ming Zhang,[g] Wenyan Su,[ahi] Wenhong Peng,[aj] Chunfeng Zhang,[f] Feng Liu,[g] Lintao Hou,[h] Weiguo Zhu,[j] Donghong Yu,[kl] Min Xiao,[f] Ellen Moons,[i] Fujun Zhang,*[c] Thomas D. Anthopoulos,[d] Olle Inganäs[e] and Ergang Wang*[am]*

[a] Department of Chemistry and Chemical Engineering, Chalmers University of Technology, Göteborg, SE-412 96, Sweden. E-mail: ergang@chalmers.se

[b] School of Chemistry and Chemical Engineering, Beijing Institute of Technology, Beijing 100081, China. E-mail: qsan@bit.edu.cn

[c] School of Science, Beijing Jiaotong University, Beijing 100044, China. E-mail: fjzhang@bjtu.edu.cn

[d] King Abdullah University of Science and Technology (KAUST), KAUST Solar Center (KSC), Thuwal 23955, Saudi Arabia.

[e] Biomolecular and Organic Electronics, Department of Physics, Chemistry and Biology (IFM), Linköping University, Linköping, SE-581 83, Sweden.

[f] National Laboratory of Solid State Microstructures, School of Physics, Collaborative Innovation Center of Advanced Microstructures, Nanjing University, Nanjing 210093, China.

[g] Department of Physics and Astronomy, Shanghai Jiaotong University, Shanghai 200240, China.

[h] Guangdong Provincial Key Laboratory of Optical Fiber Sensing and Communications, Guangzhou Key Laboratory of Vacuum Coating Technologies and New Energy Materials, Siyuan Laboratory, Department of Physics, Jinan University, Guangzhou 510632, China.

[i] Department of Engineering and Physics, Karlstad University, 65188 Karlstad, Sweden.

[j] School of Materials Science and Engineering, Jiangsu Key Laboratory of Environmentally Friendly Polymeric Materials, Jiangsu Engineering Laboratory of Light-Electricity-Heat Energy-Converting Materials and Applications, Changzhou University, Changzhou 213164, China.

[k] Department of Chemistry and Bioscience, Aalborg University, DK-9220, Aalborg, Denmark.

[l] Sino-Danish Center for Education and Research, Aarhus, DK-8000, Denmark.

[m] School of Materials Science and Engineering, Zhengzhou University, Zhengzhou 450001, China.

Materials: Y5 was synthesized according to the reference.[1] PBDB-T was purchased from Solarmer Materials Inc. Y5-Br and PF5-Y5 were synthesized in this study, the detailed synthetic procedures and characterizations of the chemical structures were summarized in Supplementary Information, as following:

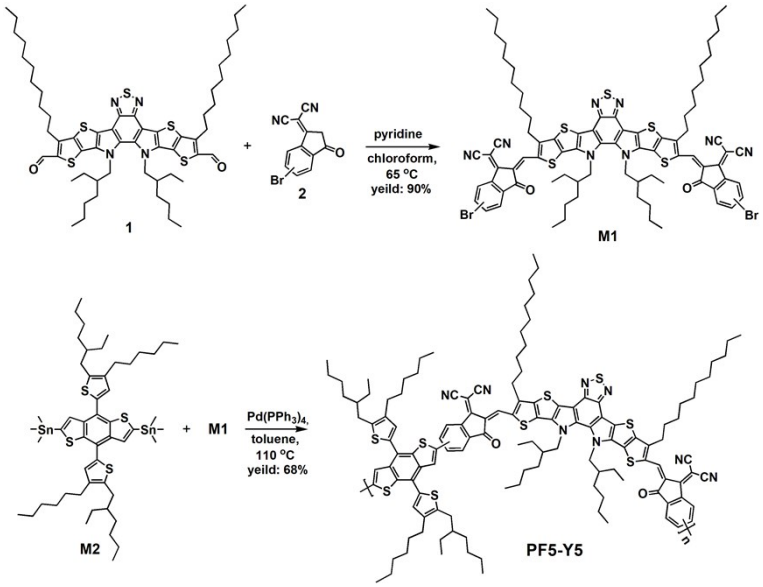

Scheme S1 The synthetic routes of polymer acceptor PF5-Y5.

Y5-Br (M1): In a dry 50 mL flask, compounds 1 (1.00 g, 0.97 mmol), 2 (1.06 g, 3.89 mmol), and pyridine (1 mL) were added to 100 mL of degassed $CHCl_3$ under nitrogen and stirred vigorously at 65 °C for 10 h. Then the mixture was poured into methanol (300 mL) followed by precipitation, and the sediments were collected. The resulting crude compound was purified by silica gel to give a black solid as M1 (1.34 g, 90%). ^{1}H NMR (400 MHz, $CDCl_3$, TMS), (ppm): (d, J = 3.1 Hz, 2H), 8.82 (d, J = 1.1 Hz, 1H), 8.55 (d, J = 8.4 Hz, 1H), 8.05 (d, J = 1.8 Hz, 0.8H), 7.90-7.83 (m, 2H), 7.80 (d, J = 7.9 Hz, 1.2H), 4.78 (d, J = 7.7 Hz, 4H), 3.22 (t, J = 7.8 Hz, 4H), 2.11 (dt, J = 12.7, 6.4 Hz, 2H), 1.93-1.82 (m, 4H), 1.53-1.43 (m, 4H), 1.43-1.12 (m, 24H), 1.13-0.94 (m, 8H), 0.86 (t, J = 6.8 Hz, 6H), 0.81-0.71 (m, 6H), 0.67 (t, J = 5.8 Hz, 6H). MALDI-TOF MS (m/z) for $C_{82}H_{88}Br_2N_8O_2S_5$, Calcd: 1537.8, Found: 1536.5.

PF5-Y5 (PF5-Y5$_{\mathbf{high}}$): In a dry 50 mL flask, $Pd(PPh_3)_4$ (18 mg) was added to a solution of M1 (Y5-Br, 200 mg, 0.13 mmol) and M2 (BDT-T-Sn, 139 mg, 0.13 mmol) in 11 mL degassed

toluene under nitrogen and stirred vigorously at 110 °C for 6 h until the reaction system became viscous. Then the mixture was poured into methanol (100 mL) for precipitation. The polymer was dissolved in chloroform and the solution was filtered through a silica gel column. The collected chloroform solution was concentrated and precipitated in methanol to get a dark solid (188 mg, 68%). Anal. Calcd for $C_{128}H_{154}N_8O_2S_9$ (%): C, 72.34; H, 7.30. Found (%): C, 72.19; H, 8.38. M_w = 33.3 kDa, PDI = 4.25.

PF5-$Y5_{low}$ and PF5-$Y5_{medium}$ were synthesized according to the above method with different reaction time of 4 h and 5 h, respectively. PF5-$Y5_{low}$: M_w = 16.5 kDa, PDI = 2.10; and PF5-$Y5_{medium}$: M_w = 25.6 kDa, PDI = 1.96.

General measurements and characterization. ^{1}H NMR spectrum was measured in $CDCl_3$ on Bruker AV 400 MHz FT-NMR spectrometer. MALDI-TOF were obtained with a Shimadzu QP2010 spectrometer. Elemental analysis was carried out on a flash EA1112 analyser. GPC measurement was carried out on Agilent Technologies PL-GPC-220 at 150 ºC, with 1,2,4-tricholorobenzene as the eluent and polystyrene as the standard. UV-vis absorption spectrum was recorded on a UV-Vis-NIR Spectrophotometer of Agilent Technologies Cary Series. AFM measurements were performed on Nanoscope Multimode 8 (Bruker, USA) in Peak Force Tapping mode (ScanAsyst), controlled by Nanoscope 9.2 software, using a Si tip in air. TEM measurement was performed using a Tecnai G2 F20 S-TWIN instrument at 200 kV accelerating voltage, in which the blend films were prepared by using a processing technique as following: firstly, the blend films were spin-cast on the PEDOT:PSS/ITO substrates; secondly, the resulting blend film/PEDOT:PSS/ITO substrates were submerged in deionized water to make these blend films float onto the air-water interface; finally, the floated blend films were taken up on unsupported 200 mesh copper grids for a TEM measurement. GIWAXS measurement was performed at beamline 7.3.3 at the Advanced Light Source with a resonant

photon energy of 284.2 eV. Samples were prepared on Si substrates using identical blend solutions as those used in devices. The 10 keV X-ray beam was incident at a grazing angle of 0.12°~0.16°, selected to maximize the scattering intensity from the samples. The scattered X-ray was detected using a Dectris Pilatus 2M photon counting detector. The CCL was defined as CCL = 0.9 × (2π/FWHM) (Å), where FWHM is the full width at half maximum of the corresponding diffraction peak.

Fabrication and characterization of photovoltaic devices. Solar cells with a device structure of ITO/PEDOT:PSS/active layer/PDINO or PNDIT-F3N/Al were fabricated under conditions as follows: the patterned ITO-coated glass was scrubbed by detergents and then cleaned inside an ultrasonic bath by using deionized water, acetone, and isopropyl alcohol sequentially and dried overnight in an oven. Before use, the glass substrates were treated in a UV-Ozone Cleaner for 10 min to improve its work function and clearance. A PEDOT:PSS (Heraeus Clevis P VP A 4083, purchased from H.C. Starck co. Ltd.) thin layer (30 nm) was spin-coated onto the ITO substrates by spin-coating method at 5000 round per minute (RPM) for 40 s, and then dried at 150 °C for 15 min in air. The PEDOT:PSS coated ITO substrates were fast transferred to a N_2 filled glove-box containing less than 5 ppm moisture and oxygen for further processing. The active layer materials were dissolved in chlorobenzene/1-chloronaphthalene (*v/v*, 100:2), then the mixture was stirred overnight at 80 ℃ to obtain a blend solution with a D/A weight ratio (*w/w*) of 1:0.75 and a total concentration of ~17.5 mg mL^{-1}. After cooling to room temperature, the blend solution was spun-cast on the top of the pre-heated ITO glass substrate with PEDOT:PSS layer at 80 ℃. Then the active layer was annealed at 100 ℃ for 10 min. The active layer thicknesses were ~100 nm, which were controlled by adjusting the spinning speed during the spin-coating process and measured by an Ambios Technology XP-2 stylus Profiler. The PDINO (purchased from Solarmer Inc) as interlayer was then deposited on top of the active

layer by spin-coating from a methanol solution with 0.25 vol% acetic acid and a concentration of 2 mg/mL at 5000 RPM for 30 s. When PNDIT-F3N was used as interface layer, it was deposited on top of the active layer by spin-coating from a methanol solution with a concentration of 0.5 mg mL^{-1}. Finally, 100 nm Al as the cathode was evaporated on the photosensitive layer under a pressure of ~10^{-4} Pa. The active areas of devices were 3.8 mm^2 tested at Beijing Jiaotong University and 10 mm^2 tested at King Abdullah University of Science and Technology, which were defined by the vertical overlap of ITO anode and Al cathode. The *J-V* characteristic curves of all devices were measured in the forward direction from −0.1 to 1.0 V with a scan step of 10 mV and a dwell time of 100 ms by using a Keithley 2400 Source Meter in a high-purity nitrogen-filled glove box. Photocurrent was measured under AM 1.5G illumination (100 mW cm^{-2}) by using a XES-40S2 (SAN-EI Electric Co., Ltd.) solar simulator (AAA grade, 70×70 mm^2 photobeam size), which was calibrated by standard silicon solar cells (purchased from Zolix INSTRUMENTS CO. LTD). The EQE spectra of devices were measured in air conditions by a Zolix Solar Cell Scan 100. Monochromatic light was generated from a Newport 300 W lamp source. To study the charge generation and dissociation processes of the photovoltaic devices, plots of the J_{ph} *versus* V_{eff} of the PSCs were performed. Here, J_{ph} and V_{eff} are defined as $J_{ph} = J_L - J_D$ and $V_{eff} = V_0 - V_{appl}$, respectively, where J_D and J_L are the photocurrent densities in the dark and under the illumination, and V_{appl} is the applied bias voltage and V_0 is the voltage at which $J_{ph} = 0$, respectively.[2] Usually, V_{eff} determines the electric field in the bulk region and thereby determines the carrier transport and the photocurrent extraction. At high V_{eff} values, charge carriers rapidly move toward the related electrodes with minimal recombination. The J_{ph} reaches the saturation current density (J_{sat}) at high V_{eff} ($\geq$ 4 V in this case). Under the maximum power output conditions, recombination will be strongly competing with the carrier extraction as carriers slow down due to the reduced electric field.

Charge mobility measurement by space charge-limited current (SCLC) method. The hole mobility was measured in a hole-only device composed of ITO/PEDOT:PSS/active layer/MoO_3/Ag. The electron mobility was measured in an electron-only device composed of ITO/ZnO/acceptor neat film or active layer/PDINO/Al. For the hole-only device, the active layers were spin-coated on ITO substrates covered with 40 nm PEDOT:PSS. The active layers were prepared according to the fabrication process of the PSCs. After that, MoO_3 (10 nm) and Ag (100 nm) was vacuum-deposited on the active layer as the cathode. For the electron-only device, the blend films were spin-coated on ITO substrates covered with a layer of ZnO (40 nm). The active layers were prepared according to the fabrication process of the PSCs. After that, PDINO (10 nm) and Al (100 nm) was vacuum-deposited on the active layer as the cathode. The detailed calculation processes were summarized in Supplementary Information.

The charge mobilities are generally described by the Mott-Gurney equation:[3]

$$J = \frac{9}{8}\varepsilon_r\varepsilon_0\mu\frac{V^2}{L^3} \quad (1)$$

where J is the current density, ε_0 is the permittivity of free space (8.85×10^{-14} F/cm), ε_r is the dielectric constant of used materials, μ is the charge mobility, V is the applied voltage and L is the active layer thickness. The ε_r parameter is assumed to be 3, which is a typical value for organic materials. In organic materials, charge mobility is usually field dependent and can be described by the disorder formalism, typically varying with electric field, E=V/L, according to the equation:

$$\mu = \mu_0 \exp[0.89\gamma\sqrt{\frac{V}{L}}] \quad (2)$$

where μ_0 is the charge mobility at zero electric field and γ is a constant. Then, the Mott-Gurney equation can be described by:

$$J = \frac{9}{8}\varepsilon_r\varepsilon_0\mu_0\frac{V^2}{L^3}\exp[0.89\gamma\sqrt{\frac{V}{L}}] \quad (3)$$

In this case, The charge mobilities were estimated using the following equation:

$$\ln(\frac{JL^3}{V^2}) = 0.89\gamma\sqrt{\frac{V}{L}} + \ln(\frac{9}{8}\varepsilon_r\varepsilon_0\mu_0) \quad (4)$$

FTPS and EQE_{EL} Measurement. The highly sensitive FTPS was measured with a Vertex 70 from Bruker Optics, which was equipped with a quartz tungsten halogen lamp, quartz beam-splitter and external detector option. A low-noise current amplifier (SR570) was used to amplify the photocurrent produced under illumination of the solar cells, with light modulated by the FTIR. The output voltage of the current amplifier was fed back into the external detector port of the FTIR to use the FTIR software to collect the photocurrent spectra. The EQE_{EL} was recorded with an in-house-built system comprising a Hamamatsu silicon photodiode 1010B, Keithley 2400 source meter, and Keithley 485 picometer. The detailed calculation processes of V_{oc} loss were summarized in Supplementary Information, as following:

K_B is the Boltzmann constant, T is the ambient temperature, q is the elementary charge, EQE_{PV} is the external quantum efficiency of solar cell, and EQE_{EL} is the electroluminescence efficiency, respectively.

$$\Delta V_{oc}/q = \frac{E_g}{q} - V_{oc} = \left(\frac{E_g}{q} - V_{oc}^{SQ}\right) + \left(V_{oc}^{SQ} - V_{oc}^{rad}\right) + \left(V_{oc}^{rad} - V_{oc}\right) \quad (5)$$

$$V_{oc}^{SQ} \approx \frac{k_B T}{q} \ln \frac{J_{sc}^{SQ}}{J_0^{SQ}} = \frac{k_B T}{q} ln \frac{\int_{Eg}^{+\infty} \Phi_{AM1.5G}(E)dE}{\int_{Eg}^{+\infty} B(E)dE} \quad (6)$$

$$V_{oc}^{rad} \approx \frac{k_B T}{q} ln \frac{J_{sc}}{J_0^{rad}} = \frac{k_B T}{q} ln \frac{\int_{0}^{+\infty} EQE_{PV}(E) * \Phi_{AM1.5G}(E)dE}{\int_{0}^{+\infty} EQE_{PV}(E) * B(E)dE} \quad (7)$$

$$\Delta V_3 = -\frac{k_B T}{q} \ln EQE_{EL} \quad (8)$$

$$B(E) = \frac{2\pi \quad E^2}{h^3 c^2 \quad e^{\frac{E}{k_B T a}}} \quad (9)$$

Transient absorption dynamic. Femtosecond-resolved TA spectroscopy was obtained using a home-built system. A Ti:Sapphire regenerative amplifier (Libra, Coherent) at 800 nm (with a repetition rate of 1 kHz and pulse duration of 90 fs) was employed to generate the pump and probe pulses. The wavelength-tunable pump beam was generated by an optical parametric amplifier (OperA Solo, Coherent) pumped with the regenerative amplifier. The visible/near infrared super-continuum probe beam was generated by focusing a small portion of the laser beam onto a sapphire/YAG plate. The TA signal was analyzed in term of differential transmittance ($\Delta T/T$) by a silicon CCD (S3070-1006 Hamamatsu) for the visible region and an InGaAs CCD (G11608 Hamamatsu) for the near-infrared region with a monochromator (Acton 2358 Princeton Instrument) at 1 kHz enabled by a custom-built control board from Entwicklungsbuero Stressing. Samples were measured in nitrogen atmosphere.

Table S1 Detailed parameters of acceptor materials from the GPC measurements

	M_n (kDa)	M_w (kDa)	PDI	Number of Repeating units
PF5-Y5$_{low}$	7.9	16.5	2.10	3.7
PF5-Y5$_{medium}$	13.0	25.6	1.96	6.1
PF5-Y5$_{high}$	7.8	33.3	4.25	3.7

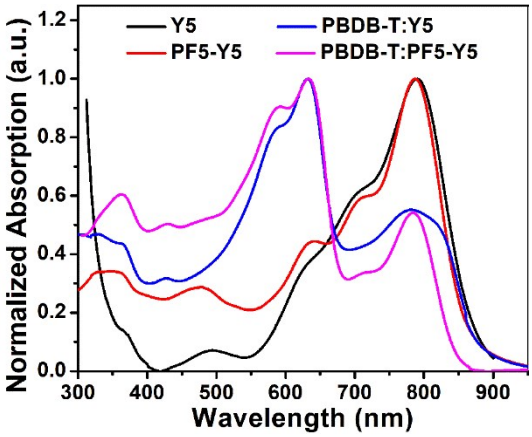

Fig. S1 The absorption spectra of the PBDB-T:Y5 and PBDB-T:PF5-Y5 blend films.

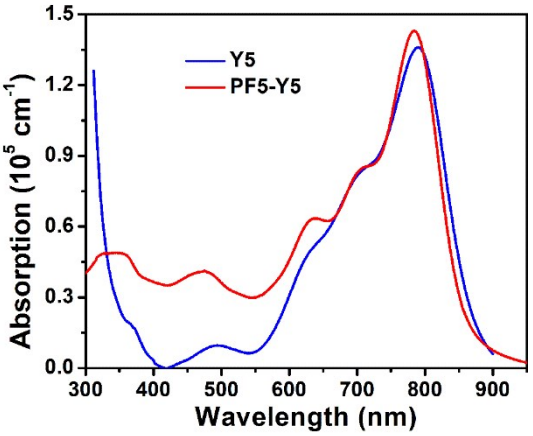

Fig. S2 The absorption spectra of Y5 and PF5-Y5 in neat films.

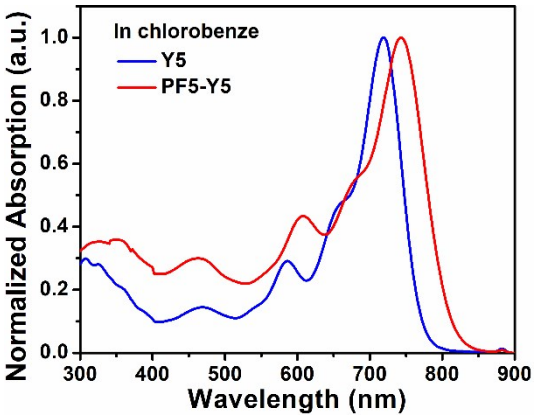

Fig. S3 The normalized absorption spectra of Y5 and PF5-Y5 in chlorobenzene solutions.

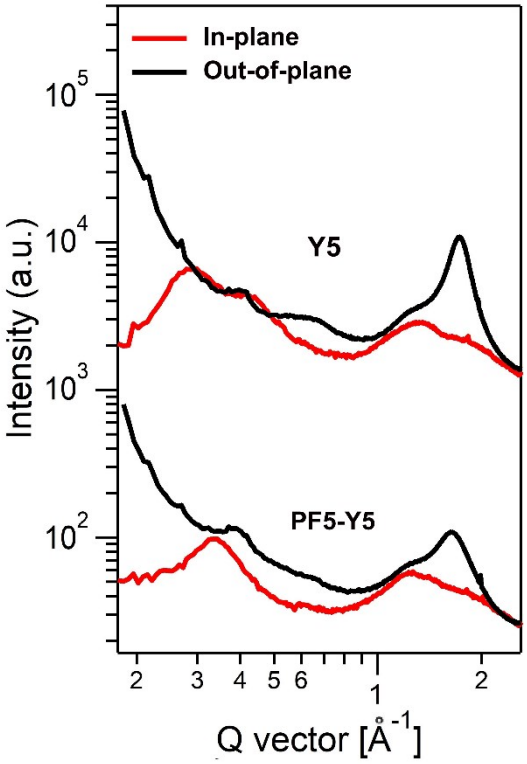

Fig. S4 The IP and OOP line-cuts of 2D GIWAXS images of Y5 and PF5-Y5 neat films.

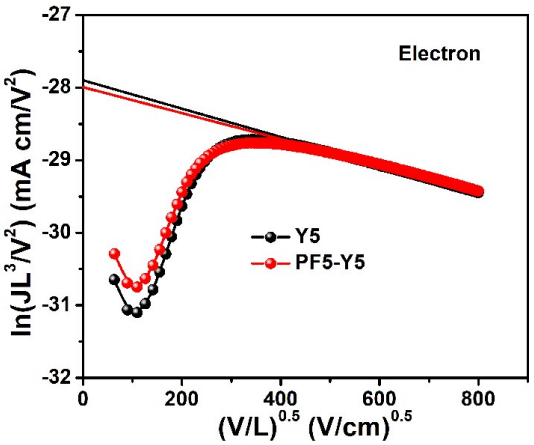

Fig. S5 The ln(JL^3/V^2) versus $(V/L)^{0.5}$ curves of the electron-only devices with a structure of ITO/ZnO/Y5 or PF5-Y5/PDINO/Al.

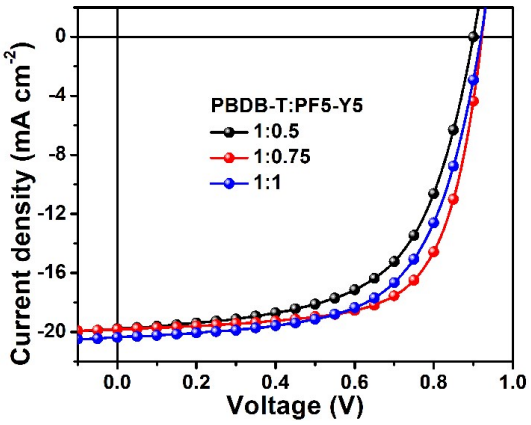

Fig. S6 The *J-V* plots of the PBDB-T:PF5-Y5-based all-PSCs with different D:A weight ratio (*w/w*) under the illumination of AM 1.5G, 100 mW cm^{-2}.

Table S2 Photovoltaic data of the PBDB-T:PF5-Y5-based all-PSCs with different D:A weight ratio (*w/w*) under the illumination of AM 1.5G, 100 mW cm^{-2}.

D:A	V_{oc} [V]	J_{sc} [mA cm^{-2}]	FF [%]	PCE [%]
1:0.5	0.905	19.78	59.8	10.71
1:0.75	0.922	19.89	67.9	12.41
1:1	0.916	20.36	62.5	11.66

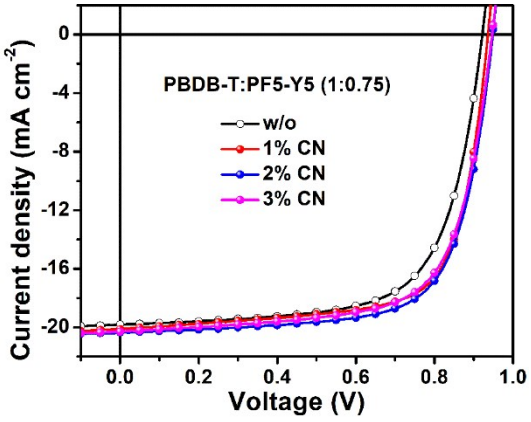

Fig. S7 The *J-V* plots of the PBDB-T:PF5-Y5 (1:0.75, *w/w*)-based all-PSCs with different CN content (*v/v*) under the illumination of AM 1.5G, 100 mW cm^{-2}.

Table S3 Photovoltaic data of the PBDB-T:PF5-Y5 (1:0.75, *w/w*)-based all-PSCs with different CN content (*v/v*) under the illumination of AM 1.5G, 100 mW cm^{-2}.

additive	V_{oc} [V]	J_{sc} [mA cm^{-2}]	FF [%]	PCE [%]
w/o	0.922	19.89	67.9	12.41
1% CN	0.937	20.20	70.2	13.28
2% CN	0.948	20.35	70.5	13.61
3% CN	0.946	20.30	68.8	13.22

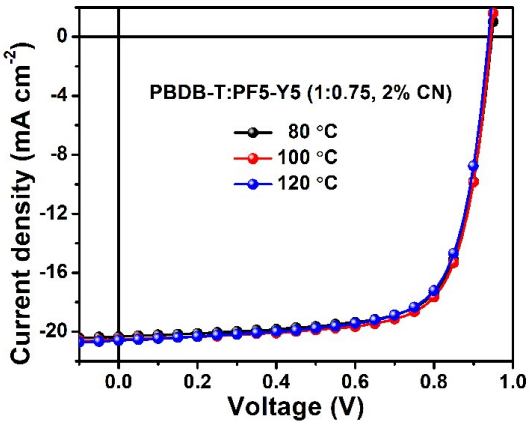

Fig. S8 The *J-V* plots of the all-PSCs based on PBDB-T:PF5-Y5 (1:0.75 in *w/w*, 2% CN in *v/v*) with different thermal annealing temperatures for 10 minutes under the illumination of AM 1.5G, 100 mW cm^{-2}.

Table S4 Photovoltaic data of the all-PSCs based on PBDB-T:PF5-Y5 (1:0.75 in *w/w*, 2% CN in *v/v*) with different thermal annealing temperatures for 10 minutes under the illumination of AM 1.5G, 100 mW cm^{-2}.

	V_{oc} [V]	J_{sc} [mA cm^{-2}]	FF [%]	PCE [%]
w/o	0.948	20.35	70.5	13.61
80 ℃	0.946	20.35	72.4	13.94
100 ℃	0.944	20.54	73.1	14.16
120 ℃	0.938	20.60	71.7	13.86

Table S5 The summaries of photovoltaic data of the all-PSCs with PCEs over 8%.

	V_{oc} [V]	J_{sc} [mA cm^{-2}]	FF [%]	PCE [%]	Ref.
PBDB-T:PF5-Y5	**0.946**	**20.65**	**74.0**	**14.46**	**This work**
PBDT-TAZ:NOE10	0.84	12.9	75	8.1	[4]
PBDB-T:N2200	0.884	12.91	75.4	8.61	[5]
PTzBI:P(NDI2OD-T2)	0.87	14.5	67.8	8.23	[6]
PCE10:D:PNDI-T10	0.84	14.4	74	9	[7]
PBDB-T:DCNBT-IDT	0.90	14.2	65	8.32	[8]
PCE10:BTI2-30TPD	1.05	13.56	58.25	8.28	[9]
PTzBI:N2200	0.87	14.72	64.1	8.21	[10]
PTzBI-O:P3F-2	0.87	14.27	63.02	8	[11]
TTFQx:T1:N2200	0.89	14.24	69	8.63	[12]
J51:N2200	0.83	14.18	70.24	8.27	[13]
PTzBI:N2200	0.84	14.86	66.65	8.36	[14]
PBDB-T:PNDI-2T-TR(10)	0.85	14.83	64.32	8.13	[15]
PBTA-Si:PTzBI-Si:N2200	0.85	14.89	75.65	9.56	[16]
PM6:PN1	1.00	15.2	69	10.5	[17]
PTzBI:N2200	0.83	15.3	70	9.1	[18]
PTzBI-Si:N2200	0.86	15.8	73	10.0	[19]
PTzBI:N2200	0.849	15.17	70.36	9.16	[20]
PTzBI-Si:N2200	0.87	15.57	73.39	10.1	[21]
PM6:PFBDT-IDTIC	0.96	15.27	68	10.3	[22]
PBDB-T:N2200	0.904	15.33	68.7	9.52	[23]
PBTA-BO:PNTB:N2200	0.84	15.77	74.98	10.09	[24]
PTB7-Th:f-BTI3-T	1.03	14.88	58.46	8.98	[25]
PBDB-T:PZ1	0.83	16.05	68.99	9.19	[26]
PTzBI-Si:N2200	0.85	16.5	77.9	11.0	[27]
PCE10:PBClT:NDP-V-C7	0.78	16.77	68.07	9.03	[28]
PTzBI-Si:N2200	0.85	17.2	77.9	11.5	[29]
PTzBI-Si:N2200	0.88	17.62	75.78	11.76	[30]
PBTA-Si:PTzBI-Si:N2200	0.82	17.52	72.1	10.4	[31]

PBDB-T:PNDIBS	0.85	18.32	57	9.38	[32]
PBDB-T:BSS10	0.86	18.55	64	10.1	[33]
PTB7-Th:NDP-V	0.74	17.07	67	8.59	[34]
PBDTS-TPD:PNDI-T	1.10	11.3	61	8	[35]
PM6:PYT	0.93	21.78	66.33	13.44	[36]
PBDB-T:PJ1	0.90	22.3	70	14.4	[37]
PM6:PF3-DTCO	0.943	15.75	68.2	10.13	[38]
PM6:PF2-DTSi	0.99	16.48	66.1	10.77	[39]
PBDB-T:A701	0.92	18.27	64	10.7	[40]
PBDB-T:PTPBT-ET	0.899	21.33	65.3	12.52	[41]

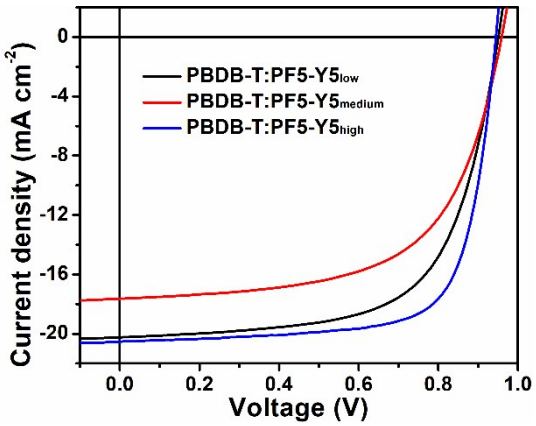

Fig. S9 The *J-V* plots of the all-PSCs based on polymer acceptors PF5-Y6 with different molecular weights under the illumination of AM 1.5G, 100 mW cm^{-2}.

Table S6 Photovoltaic data of the all-PSCs based on polymer acceptors PF5-Y6 with different molecular weights under the illumination of AM 1.5G, 100 mW cm^{-2}.

	M_w (kDa)	V_{oc} [V]	J_{sc} [mA cm^{-2}]	FF [%]	PCE [%]
PF5-Y5$_{low}$	16.5	0.951	20.24	64.6	12.41
PF5-Y5$_{medium}$	25.6	0.959	17.64	60.8	10.28
PF5-Y5$_{high}$	33.3	0.946	20.65	74.0	14.45

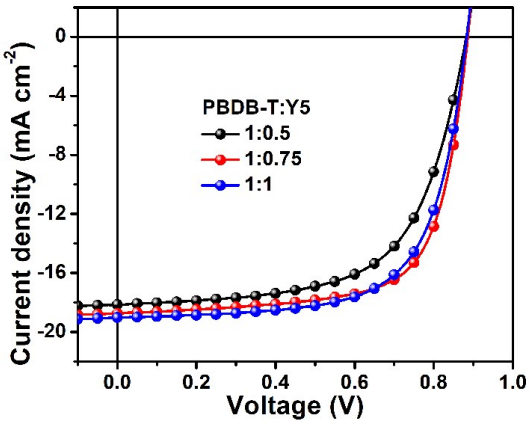

Fig. S10 The *J-V* plots of the PBDB-T:Y5-based all-PSCs with different D:A weight ratio (*w/w*) under the illumination of AM 1.5G, 100 mW cm^{-2}.

Table S7 Photovoltaic data of the PBDB-T:Y5-based all-PSCs with different D:A weight ratio (*w/w*) under the illumination of AM 1.5G, 100 mW cm^{-2}.

D:A	V_{oc} [V]	J_{sc} [mA cm^{-2}]	FF [%]	PCE [%]
1:0.5	0.882	18.14	62.6	10.02
1:0.75	0.886	18.74	69.8	11.59
1:1	0.883	19.02	67.2	11.29

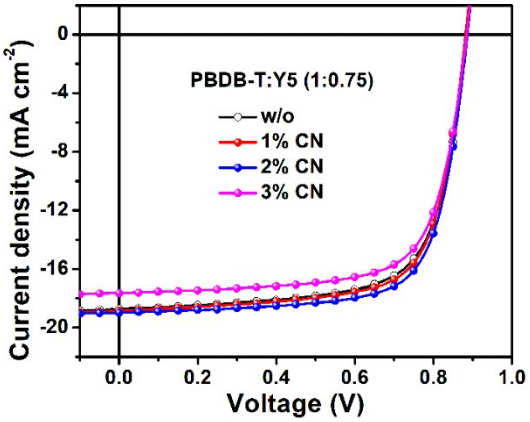

Fig. S11 The *J-V* plots of the PBDB-T:Y5 (1:0.75, *w/w*)-based all-PSCs with different CN content (*v/v*) under the illumination of AM 1.5G, 100 mW cm^{-2}.

Table S8 Photovoltaic data of the PBDB-T:Y5 (1:0.75, *w/w*)-based all-PSCs with different CN content (*v/v*) under the illumination of AM 1.5G, 100 mW cm^{-2}.

	V_{oc} [V]	J_{sc} [mA cm^{-2}]	FF [%]	PCE [%]
w/o	0.886	18.74	69.8	11.59
1% CN	0.886	18.82	70.6	11.78
2% CN	0.886	18.98	72.2	12.15
3% CN	0.883	18.35	70.9	11.48

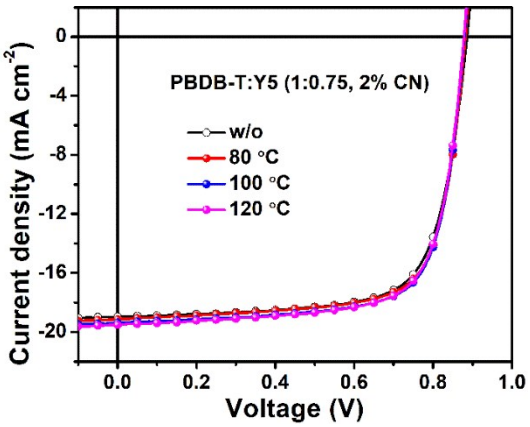

Fig. S12 The *J-V* plots of the all-PSCs based on PBDB-T:Y5 (1:0.75 in *w/w*, 2% CN in *v/v*) with different thermal annealing temperatures for 10 minutes under the illumination of AM 1.5G, 100 mW cm^{-2}.

Table S9 Photovoltaic data of the all-PSCs based on PBDB-T:Y5 (1:0.75 in *w/w*, 2% CN in *v/v*) with different thermal annealing temperatures for 10 minutes under the illumination of AM 1.5G, 100 mW cm^{-2}.

	V_{oc} [V]	J_{sc} [mA cm^{-2}]	FF [%]	PCE [%]
w/o	0.886	18.98	72.2	12.15
80 ℃	0.882	19.15	73.0	12.33
100 ℃	0.880	19.38	73.4	12.52
120 ℃	0.878	19.52	72.7	12.45

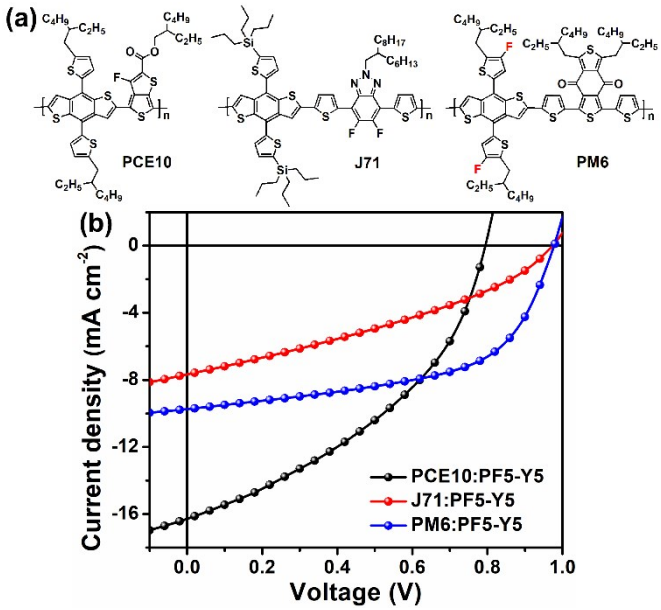

Fig. S13 (a) Molecular structures of the other model polymer donors of PCE10, J71, and PM6. (b) The *J*-*V* plots of the PF5-Y5-based all-PSCs with different polymer donors under the illumination of AM 1.5G, 100 mW cm^{-2}.

Table S10 Summary of key photovoltaic parameters of the PF5-Y5-based all-PSCs with different polymer donors under the illumination of AM 1.5G, 100 mW cm^{-2}.

Active layers	V_{oc} [V]	J_{sc} [mA cm^{-2}]	FF [%]	PCE [%]
PCE10:PF5-Y5	0.807	16.29	39.8	5.23
J71:PF5-Y5	0.979	7.67	34.2	2.57
PM6:PF5-Y5	0.980	9.74	56.2	5.37

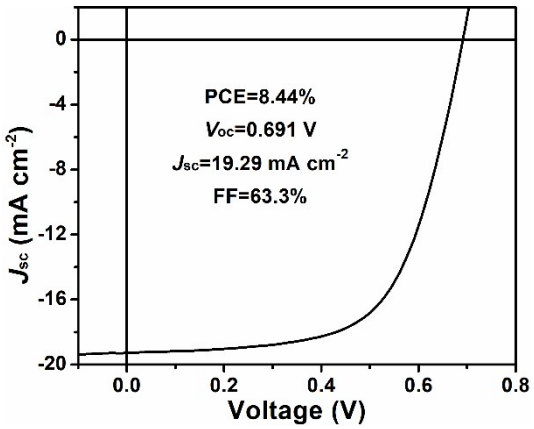

Fig. S14 The *J*-*V* plot of the PBDB-T:Y6-based PSCs based on under the illumination of AM 1.5G, 100 mW cm^{-2}.

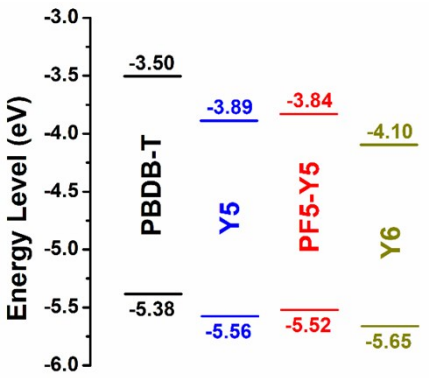

Fig. S15 Molecular energy level diagrams of the acceptor and donor photovoltaic materials in neat films using cyclic voltammetry.

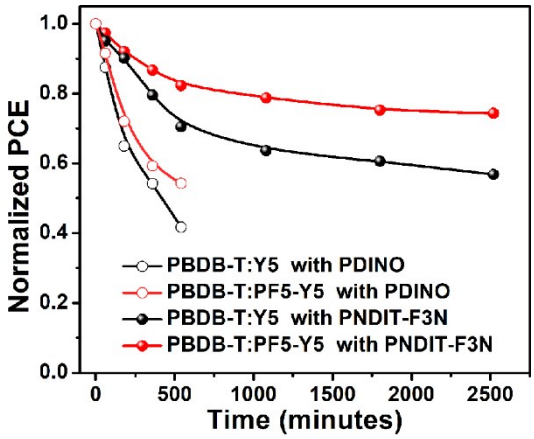

Fig. S16 Thermal stability of the devices with different interface layers along annealing temperature of 85 °C in N_2 atmosphere under dark.

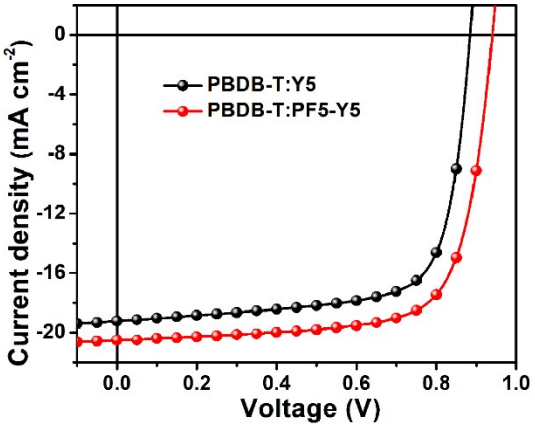

Fig. S17 The *J-V* plots of the PBDB-T:Y5-based and PBDB-T:PF5-Y5-based devices with PNDIT-F3N as interface layer under the illumination of AM 1.5G, 100 mW cm^{-2}.

Table S11 Summary of key photovoltaic parameters of the PBDB-T:Y5-based and PBDB-T:PF5-Y5-based devices with PNDIT-F3N as interface layer under the illumination of AM 1.5G, 100 mW cm^{-2}.

Active layers	V_{oc} [V]	J_{sc} [mA cm^{-2}]	FF [%]	PCE [%]
PBDB-T:Y5	0.885	19.22	72.8	12.38
PBDB-T:PF5-Y5	0.940	20.51	72.7	14.01

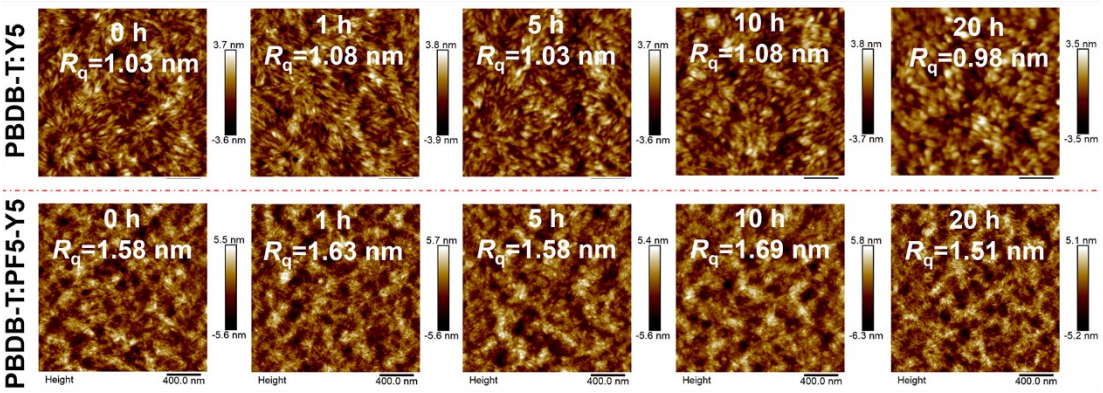

Fig. S18 AFM images of the PBDB-T:Y5 blends (above) and the PBDB-T:PF5-Y5 blends (below) with different annealing time at 85 °C in the N_2-filled glove box under dark.

Table S12 Data summaries of the PBDB-T:Y5- and PBDB-T:PF5-Y5-based PSCs.

Active layers	J_{sat} [mA cm^{-2}]	J_{ph}^{*} [mA cm^{-2}]	$J_{ph}^{\&}$ [mA cm^{-2}]	J_{ph}^{*}/J_{sat} [%]	$J_{ph}^{\&}/J_{sat}$ [%]
PBDB-T:Y5	20.61	19.38	16.85	94.03	81.76
PBDB-T:PF5-Y5	21.62	20.54	18.17	95.00	84.04

J_{sat}: The J_{ph} under condition of V_{eff}=4.0 V; J_{ph}^{*}: The J_{ph} under short-circuit condition; $J_{ph}^{\&}$: The J_{ph} under maximum power output condition.

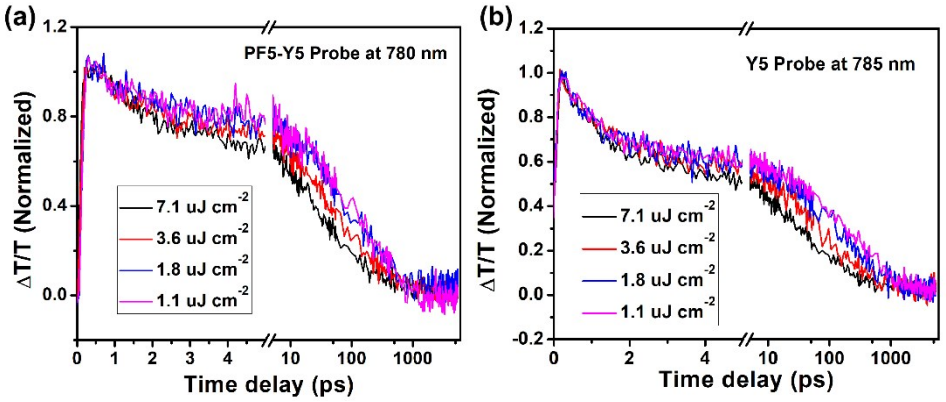

Fig. S19 Femtosecond-resolved transient absorption dynamic curves probed at (a) 780 nm from the PF5-Y5 pure film and (b) 785 nm from the Y5 pure film with different excitation intensities.

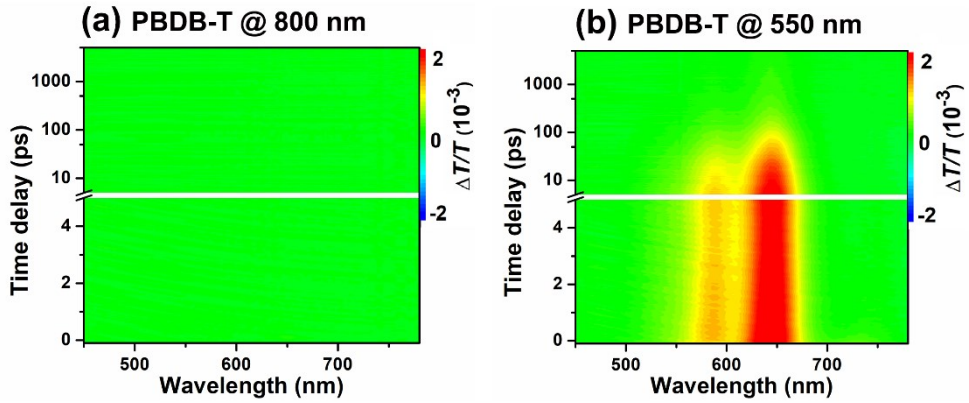

Fig. S20 Transient absorption signal recorded from PBDB-T neat film excited at (a) 800 nm and (b) 550 nm.

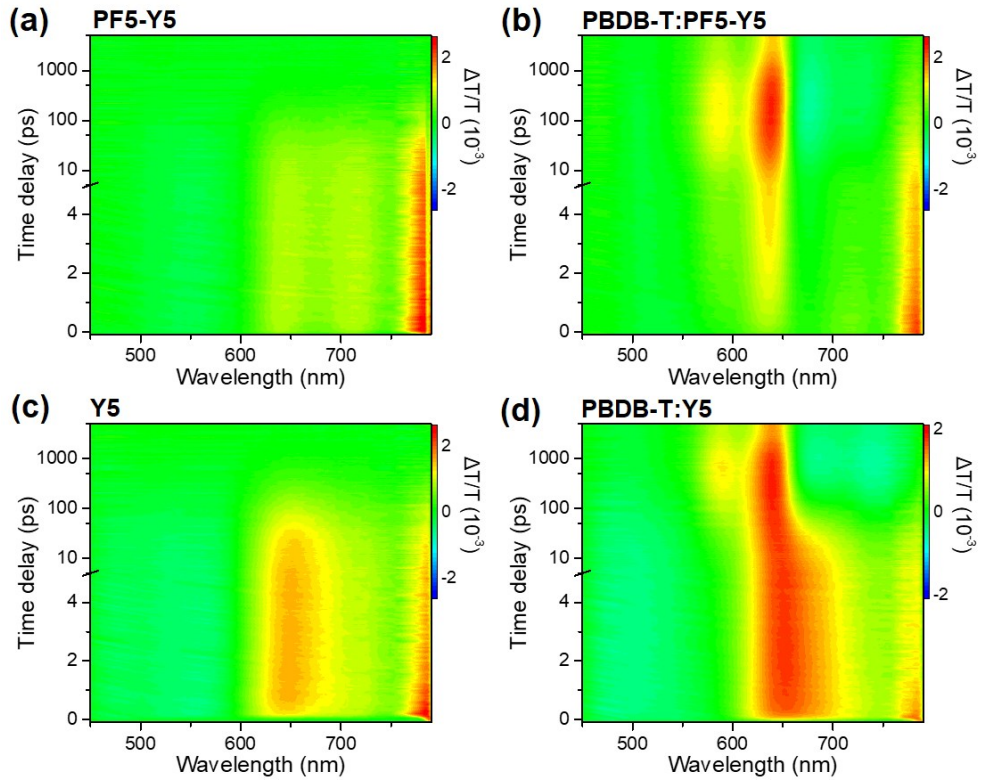

Fig. S21 Transient absorption signal recorded from (a) PF5-Y5 and (c) Y5 neat films, as well as (b) PBDB-T:PF5-Y5 and (d) PBDB-T:Y5 blend films excited at 800 nm.

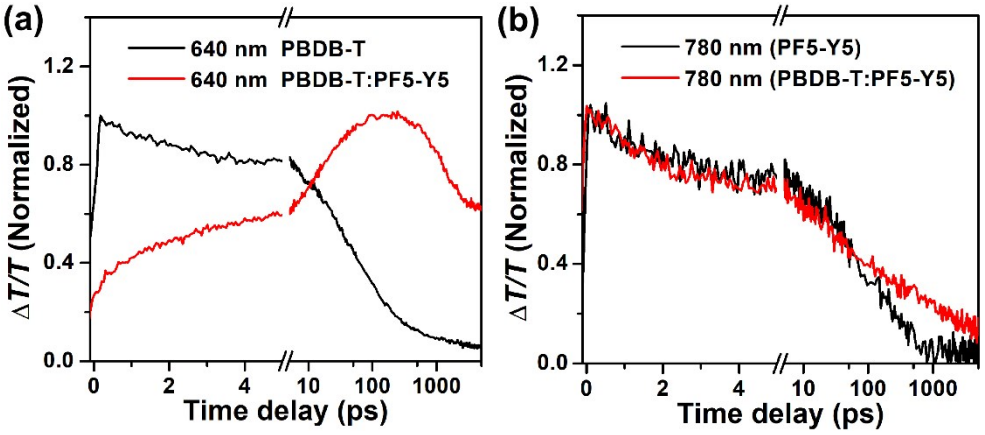

Fig. S22 Femtosecond-resolved transient absorption dynamic curves probed at (a) 640 nm from the PBDB-T pure film and PBDB-T:PF5-Y5 blend film, as well as (b) 780 nm from the PF5-Y5 pure film and PBDB-T:PF5-Y5 blend film.

Table S13 GIWAXS test performance parameters of the Y5 and PF5-Y5 pure films and the related blend films.

	in plane			out of plane		
	location ($Å^{-1}$)	d-spacing (Å)	CCL (Å)	location ($Å^{-1}$)	d-spacing (Å)	CCL (Å)
PBDB-T	0.30	21.24	57.32	1.70	3.69	14.93
Y5	0.29	21.99	46.51	1.73	3.64	20.34
PF5-Y5	0.34	18.56	45.93	1.65	3.82	12.70
PBDB-T:Y5	0.30	21.23	124.0	1.73	3.63	19.16
PBDB-T:PF5-Y5	0.30[a]	21.27	139.7	1.69	3.72	18.04
	0.33[b]	19.10	43.39			

(100) diffraction peak in IP direction attributed from [a]PBDB-T and [b]PF5-Y5. It should be noted that (100) peaks of PBDB-T and Y5 in blends could not be separated since the positions of these two peaks are too close.

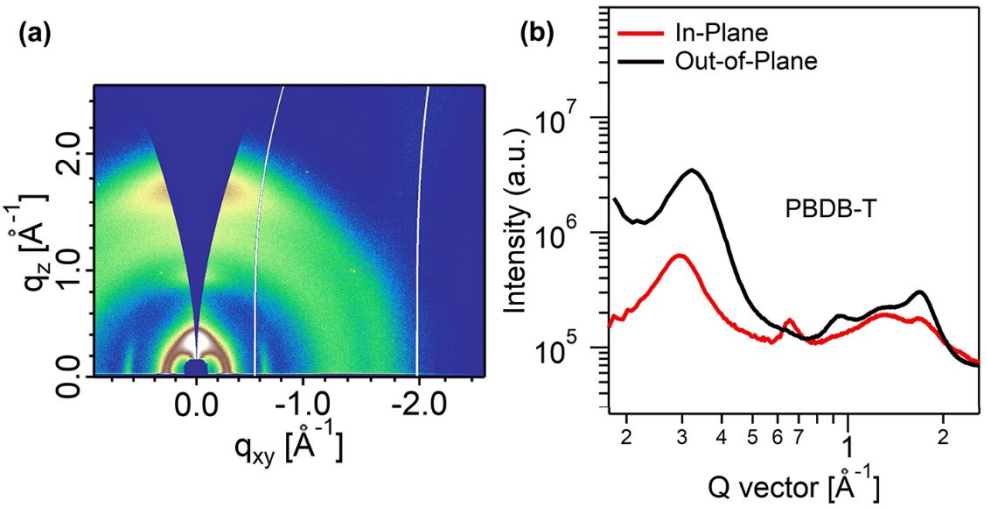

Fig. S23 (a) The 2D GIWAXS profile and (b) the corresponding IP and OOP line-cuts of the polymer donor PBDB-T neat film.

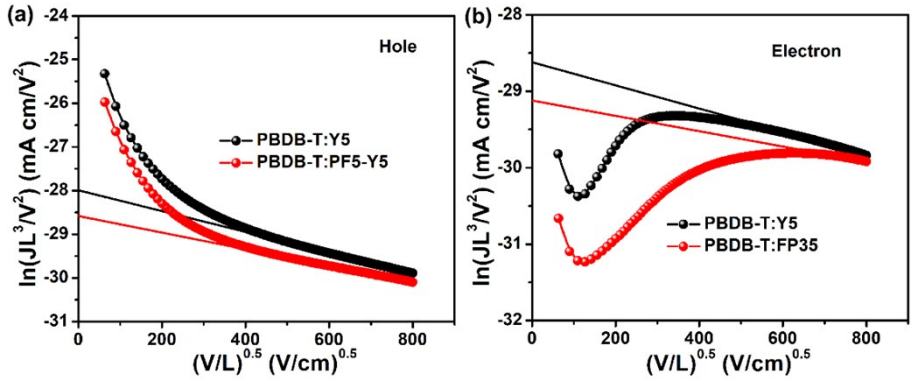

Fig. S24 (a) The *J-V* curves of the hole-only devices with a structure of ITO/PEDOT:PSS/active layer/MoO_3/Ag and (b) the electron-only devices with a structure of ITO/ZnO/active layer/PDINO/Al.

Table S14 Data summaries of the charge mobilities of the devices based on pure acceptor films and/or the corresponding blend films.

	μ_e [10^{-3} cm^2 V^{-1} s^{-1}]	μ_h [10^{-3} cm^2 V^{-1} s^{-1}]	μ_h/μ_e
Y5	3.82 (3.11±0.52)	-	-
PF5-Y5	3.18 (2.70±0.37)	-	-
PBDB-T:Y5	1.23 (1.02±0.13)	2.32 (1.81±0.38)	1.89
PBDB-T:PF5-Y5	0.76 (0.65±0.08)	1.30 (1.08±0.18)	1.71

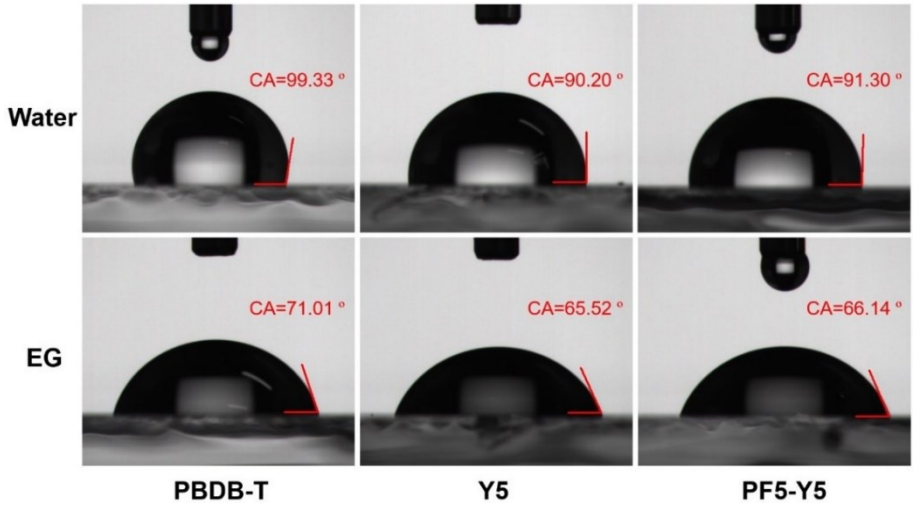

Fig. S25 Contact angle images of pure PBDB-T, Y5, and PF5-Y5 films on water and ethylene glycol (EG).

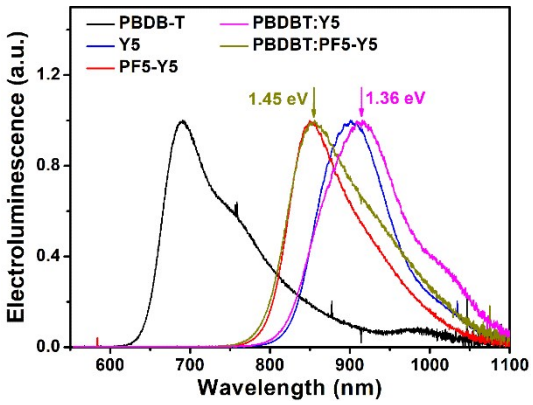

Fig. S26 Electroluminescence for donor and acceptor neat films and related blend films.

Notes and references

1. J. Yuan, Y. Zhang, L. Zhou, C. Zhang, T.-K. Lau, G. Zhang, X. Lu, H.-L. Yip, S. K. So, S. Beaupré, M. Mainville, P. A. Johnson, M. Leclerc, H. Chen, H. Peng, Y. Li and Y. Zou, *Adv. Mater.*, 2019, **31**, 1807577.

2. P. W. M. Blom, V. D. Mihailetchi, L. J. A. Koster and D. E. Markov, *Adv. Mater.*, 2007, **19**, 1551.

3. V. D. Mihailetchi, P. W. M. Blom, J. C. Hummelen and M. T. Rispens, *J. App. Phys.*, 2003, **94**, 6849.

4. X. Liu, C. Zhang, C. Duan, M. Li, Z. Hu, J. Wang, F. Liu, N. Li, C. J. Brabec, R. A. J. Janssen, G. C. Bazan, F. Huang and Y. Cao, *J. Am. Chem. Soc.*, 2018, **140**, 8934.

5. X. Liu, Y. Zou, H.-Q. Wang, L. Wang, J. Fang and C. Yang, *ACS Appl. Mater. Interfaces*, 2018, **10**, 38302.

6. J. Yuan, Y. Xu, G. Shi, X. Ling, L. Ying, F. Huang, T. H. Lee, H. Y. Woo, J. Y. Kim, Y. Cao and W. Ma, *J. Mater. Chem. A*, 2018, **6**, 10421.

7. Z. Li, X. Xu, W. Zhang, X. Meng, Z. Genene, W. Ma, W. Mammo, A. Yartsev, M. R. Andersson, R. A. J. Janssen and E. Wang, *Energy Environ. Sci.*, 2017, **10**, 2212.

8. S. Shi, P. Chen, Y. Chen, K. Feng, B. Liu, J. Chen, Q. Liao, B. Tu, J. Luo, M. Su, H. Guo, M.-G. Kim, A. Facchetti and X. Guo, *Adv. Mater.*, 2019, **31**, 1905161.

9. H. Sun, B. Liu, C. W. Koh, Y. Zhang, J. Chen, Y. Wang, P. Chen, B. Tu, M. Su, H. Wang, Y. Tang, Y. Shi, H. Y. Woo and X. Guo, *Adv. Funct. Mater.*, 2019, **29**, 1903970.

10. Y. Xu, J. Yuan, S. Zhou, M. Seifrid, L. Ying, B. Li, F. Huang, G. C. Bazan and W. Ma, *Adv. Funct. Mater.*, 2019, **29**, 1806747.

11. K. Li, R. Xie, W. Zhong, K. Lin, L. Ying, F. Huang and Y. Cao, *Sci. China Chem.*, 2018, **61**, 576.

12. L. Zhou, T.-K. Lau, H. Peng, B. Qiu, L. Jiang, X. Lu, G. Zhang, J. Yuan, Y. Li and Y. Zou, *Sol. RRL*, 2019, **3**, 1800340.

13. L. Gao, Z.-G. Zhang, L. Xue, J. Min, J. Zhang, Z. Wei and Y. Li, *Adv. Mater.*, 2016, **28**, 1884.

14. B. Lin, L. Zhang, H. Zhao, X. Xu, K. Zhou, S. Zhang, L. Gou, B. Fan, L. Zhang, H. Yan, X. D. Gu, L. Ying, F. Huang, Y. Cao and W. Ma, *Nano Energy*, 2019, **59**, 277.

15. D. Chen, J. Yao, L. Chen, J. Yin, R. Lv, B. Huang, S. Liu, Z. Zhang, C. Yang, Y. Chen and Y. Li, *Angew. Chem. Int. Ed.*, 2018**, 57**, 4580.

16. B. Fan, P. Zhu, J. Xin, N. Li, L. Ying, W. Zhong, Z. Li, W. Ma, F. Huang and Y. Cao, *Adv. Energy Mater.*, 2018, **8**, 1703085.

17. J. Wu, Y. Meng, X. Guo, L. Zhu, F. Liu and M. Zhang, *J. Mater. Chem. A*, 2019, **7**, 16190.

18. W. Zhong, Q. Hu, Y. Jiang, Y. Li, T. L. Chen, L. Ying, F. Liu, C. Wang, Y. Liu, F. Huang, Y. Cao and T. P. Russell, *Sol. RRL*, 2019, **3**, 1900032.

19. K. Zhang, R. Xia, B. Fan, X. Liu, Z. Wang, S. Dong, H.-L. Yip, L. Ying, F. Huang and Y. Cao, *Adv. Mater.*, 2018, **30**, 1803166.

20. B. Fan, L. Ying, Z. Wang, B. He, X.-F. Jiang, F. Huang and Y. Cao, *Energy Environ. Sci.*, 2017, **10**, 1243.

21. B. Fan, L. Ying, P. Zhu, F. Pan, F. Liu, J. Chen, F. Huang and Y. Cao, *Adv. Mater.*, 2017, **29**, 1703906.

22. H. Yao, F. Bai, H. Hu, L. Arunagiri, J. Zhang, Y. Chen, H. Yu, S. Chen, T. Liu, J. Y. L. Lai, Y. Zou, H. Ade and H. Yan, *ACS Energy Lett.*, 2019, **4**, 417.

23. Y. Xu, J. Yuan, S. Liang, J.-D. Chen, Y. Xia, B. W. Larson, Y. Wang, G. M. Su, Y. Zhang, C. Cui, M. Wang, H. Zhao and W. Ma, *ACS Energy Lett.*, 2019, **4**, 2277.

24. Z. Li, R. Xie, W. Zhong, B. Fan, J. Ali, L. Ying, F. Liu, N. Li, F. Huang and Y. Cao, *Sol. RRL*, 2018, **2**, 1800196.

25. Y. Wang, Z. Yan, M. A. Uddin, X. Zhou, K. Yang, Y. Tang, B. Liu, Y. Shi, H. Sun, A. Deng, J. Dai, H. Y. Woo and X. Guo, *Sol. RRL*, 2019, **3**, 1900107.

26. Z.-G. Zhang, Y. Yang, J. Yao, L. Xue, S. Chen, X. Li, W. Morrison, C. Yang and Y. Li, *Angew. Chem. Int. Ed.*, 2017, **129**, 13688.

27. Z. Li, L. Ying, P. Zhu, W. Zhong, N. Li, F. Liu, F. Huang and Y. Cao, *Energy Environ. Sci.*, 2019, **12**, 157.

28. H. Chen, Y. Guo, P. Chao, L. Liu, W. Chen, D. Zhao and F. He, *Sci. China Chem.*, 2019, **62**, 238.

29. Z. Li, W. Zhong, L. Ying, F. Liu, N. Li, F. Huang and Y. Cao, *Nano Energy*, 2019, **64**, 103931.

30. L. Zhu, W. Zhong, C. Qiu, B. Lyu, Z. Zhou, M. Zhang, J. Song, J. Xu, J. Wang, J. Ali, W. Feng, Z. Shi, X. Gu, L. Ying, Y. Zhang and F. Liu, *Adv. Mater.*, 2019, **31**, 1902899.

31. B. Fan, W. Zhong, L. Ying, D. Zhang, M. Li, Y. Lin, R. Xia, F. Liu, H. L. Yip, N. Li, Y. Ma, C. J. Brabec, F. Huang and Y. Cao, *Nat. Commun.*, 2019, **10**, 4100.

32. N. B. Kolhe, H. Lee, D. Kuzuhara, N. Yoshimoto, T. Koganezawa and S. A. Jenekhe, *Chem. Mater.*, 2018, **30**, 6540.

33. N. B. Kolhe, D. K. Tran, H. Lee, D. Kuzuhara, N. Yoshimoto, T. Koganezawa and S. A. Jenekhe, *ACS Energy Lett.*, 2019, **4**, 1162.

34. Y. Guo, Y. Li, O. Awartani, H. Han, J. Zhao, H. Ade, H. Yan and D. Zhao, *Adv. Mater.*, 2017, **29**, 1700309.

35. X. Xu, Z. Li, W. Zhang, X. Meng, X. Zou, D. D. C. Rasi, W. Ma, A. Yartsev, M. R. Andersson, R. A. J. Janssen and E. Wang. *Adv. Energy Mater.*, 2018, **8**, 1700908.

36. W. Wang, Q. Wu, R. Sun, J. Guo, Y. Wu, M. Shi, W. Yang, H. Li and J. Min, *Joule*, 2020, **4**, 1070.

37. T. Jia, J. Zhang, W. Zhong, Y. Liang, K. Zhang, S. Dong, L. Ying, F. Liu, X. Wang, F. Huang and Y. Cao, *Nano Energy*, 2020, **72**, 104718.

38. Q. Fan, R. Ma, T. Liu, W. Su, W. Peng, M. Zhang, Z. Wang, X. Wen, Z. Cong, Z. Luo, L. Hou, F. Liu, W. Zhu, D. Yu, H. Yan and E. Wang, *Solar RRL*, 2020, 10.1002/solr.202000142.

39. Q. Fan, W. Su, S. Chen, W. Kim, X. Chen, B. Lee, T. Liu, U. A. Méndez-Romero, R. Ma, T. Yang, W. Zhuang, Y. Li, Y. Li, T.-S. Kim, L. Hou, C. Yang, H. Yan, D. Yu and E. Wang, *Joule*, 2020, **4**, 658.

40. A. Tang, J. Li, B. Zhang, J. Peng and E. Zhou, *ACS Macro Lett.*, 2020, **9**, 706

41. J. Du, K. Hu, L. Meng, I. Angunawela, J. Zhang, S. Qin, A. Liebman-Pelaez, C. Zhu, Z. Zhang, H. Ade and Y. Li, *Angew. Chem. Int. Ed.*, 2020, DOI: 10.1002/anie.202005357.